Journal of Alloys and Compounds 480 (2009) 225–229

Contents lists available at ScienceDirect

Journal of Alloys and Compounds

journal homepage: www.elsevier.com/locate/jallcom

Structural and magnetic properties of Ni_3N synthesized by multidipolar microwave plasma-assisted reactive sputtering

D. Vempaire[a,b,1], S. Miraglia[a], J. Pelletier[b], D. Fruchart[a,*], E.K. Hlil[a], L. Ortega[a], A. Sulpice[a], F. Fettar[a]

[a] Institut Néel, CNRS, BP 166, 38042 Grenoble Cedex 9, France
[b] Centre de Recherche Plasmas-Matériaux-Nanostructures, LPSC, 38026 Grenoble Cedex 9, France

ARTICLE INFO

Article history:
Received 4 February 2009
Received in revised form 17 February 2009
Accepted 19 February 2009
Available online 4 March 2009

Keywords:
Magnetic layers
Nickel nitrides
Plasma-assisted deposit

ABSTRACT

Nickel nitride layers have been synthesized by using microwave plasma-assisted reactive sputtering. In the Ar–N_2 mixture used for the deposition, the Ar partial pressure was kept constant (0.015 Pa) and the N_2 pressure $p(N_2)$ was chosen between 0.014 and 0.045 Pa. The reactive sputtering assisted by microwave multidipolar plasma appears to be a powerful technique for tailoring the stoichiometry of transition metal nitrides. Physical measurements performed on a stoichiometric nickel nitride Ni_3N film deposited prove the non-ferromagnetic behavior of this compound.

1. Introduction

Transition metal nitrides have received increasing attention in recent years due to their outstanding mechanical, optical, electrical and magnetic properties. For instance, these materials can be used for corrosion resistant [1] and optical [2] coatings, electrical contacts [3] and diffusion barriers [4]. Another interesting goal is the change of magnetic properties (coercivity, magnetic moment) by the insertion of nitrogen atoms in such metal materials [5]. In this recent reference, high saturation magnetization with high electric resistance levels has been reported to take place in the Fe–N system, suggesting interesting high-frequency magnetic applications.

However, if the Fe–N system was extensively studied during last decades, only a few investigations concern with the parent Ni–N system. This is due, in particular, to the difficulty to synthesize the corresponding nickel nitrides, which are known especially metastable. Thus, the Ni–N phase diagram presents only few well-identified phases comparison made with the Fe–N system. There are only two nickel nitrides known to be rather stable at room temperature, the hcp Ni_3N (space group $P6_322$) [6] and the bct Ni_2N (SG $I4/mmm$) [7]. Effectively, in the recent literature [8,9] only a few studies demonstrate ability to synthesize pure Ni_3N, usually by using nitrogen implantation in nickel layers. However, for most of these reports, the materials appear as mixtures of various nitride phases [10–12] or contain residual Ni metal, which do not allow in both cases accurate characterizations of the physical properties. For instance, it was reported that Ni_3N exhibits a ferromagnetic component, with a weak saturation magnetization as low as 7–10 emu/cm^3 [11–13]. Effectively, the coexistence of different nickel nitrides and possible traces of Ni metal prevent determining an estimate of the magnetic moment of Ni in Ni_3N. Consequently, the magnetic state of pure systems, either Ni_3N or Ni_2N, cannot be considered experimentally established at the present time.

Here, we report on structural and magnetic properties of different Ni_3N and Ni_2N thin films deposited by reactive sputtering assisted by multidipolar microwave plasma. After varying accurately the N_2 partial pressure in the Ar/N_2 mixture, we have been able to synthesize and then study the structural and magnetic properties of pure polycrystalline and high quality Ni_3N thin films.

2. Experimental

All Ni nitride thin layers were deposited by reactive sputtering assisted by multidipolar microwave plasma [14]. In this technique, the Ni targets and Si (1 0 0) substrate are immersed in low pressure (~0.15 Pa) microwave plasma of argon and nitrogen. A DC voltage is applied to the targets in order to sputter nickel. For such a technique, no magnets are required behind the target to confine the plasma and magnetic elements such as Ni or Fe iron can be used easily. In order to realize different experimental conditions, the N_2 partial pressure $p(N_2)$ was varied from 0.010, 0.014, 0.016, 0.018, 0.023, 0.030, 0.034, to 0.045 Pa. Interestingly, we note a total absence of target poisoning phenomenon for the Ni–N system. All other deposition parameters such as the thickness of deposit (typically 100 nm), the temperature of the substrate (maintained at 20 °C), the substrate bias voltage (floating voltage), the target DC voltage (−600 V), and the microwave source power (2500 W) were

* Corresponding author. Tel.: +33 4 76 88 11 43; fax: +33 4 76 88 10 38.
E-mail address: daniel.fruchart@grenoble.cnrs.fr (D. Fruchart).
[1] Present address: Laboratoire des Technologies de la Microélectronique, 38054 Grenoble Cedex 9, France.

0925-8388/$ – see front matter © 2009 Published by Elsevier B.V.
doi:10.1016/j.jallcom.2009.02.066

kept constant for each sample of the series. The structure analysis of the layers was performed using X-ray diffraction at $\lambda_{Fe}(K\alpha) = 1.936$ Å with a grazing incidence of about 1°. Such a low incident angle was kept fixed just above the critical angle of the layer in the aim to minimize the background due to diffraction of the substrate. Pole figure measurements were carried out using a 4-circle Seifert diffractometer at $\lambda_{Cu}(K\alpha) = 1.5418$ Å. Magnetic characteristics were measured at 4 K using a SQUID magnetometer (Quantum Device).

3. Structural properties

3.1. Crystal structure analysis

In Fig. 1 are shown normalized XRD patterns at grazing incidence for nickel nitrides deposited under a N_2 partial pressure varying from 0.014 to 0.045 Pa. The normalization was done with respect to the intensity of the Ni_3N (1 1 1) Bragg peak. For comparison, in Fig. 1 we have plotted the diffraction patterns of Ni_3N [6] and Ni_2N [7] as calculated from the respective cell parameters. The choice of Refs. [6,7] among the several ones reported in literature was made owing to their pertinent contribution to structure analysis of nickel nitrides. In the present experimental data dedicated to Ni_3N as shown in Fig. 1, no specific peak can be considered arising from a residual Ni fcc type of phase. This means that almost no amount of untransformed Ni metal is present in the nitride layers considered here. However, for syntheses realized under N_2 pressure higher than 0.034 Pa, additional diffraction lines of Ni_2N are detected from the layers. Furthermore, for much higher used N_2 partial pressure at synthesis (>0.10 Pa) Ni_2N is the unique phase forming the layer. It worth to note that all the diffraction patterns presented in Fig. 1 show a relative peak intensity distribution, markedly different from

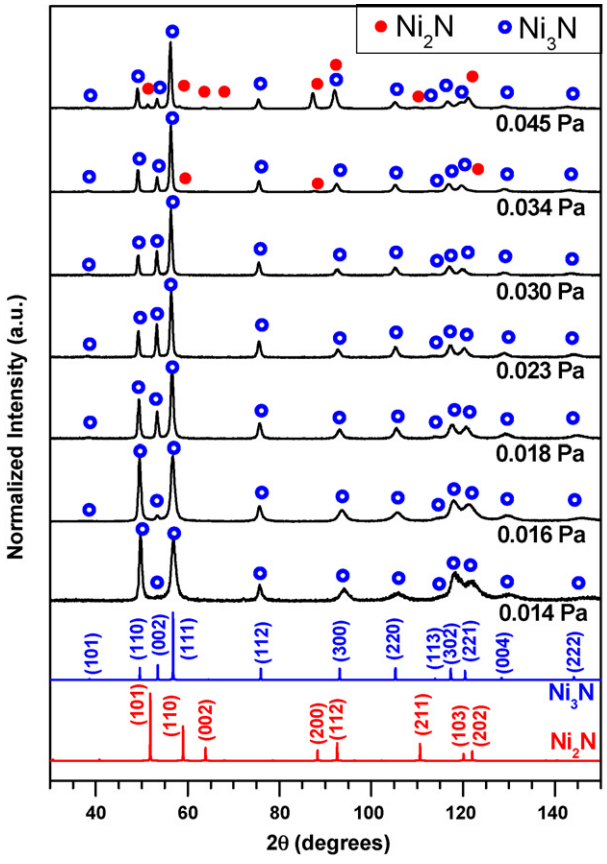

Fig. 1. Grazing incidence X-ray diffraction patterns (in normalized intensities, λ = 1.936 Å) of nickel nitrides elaborated under different nitrogen partial pressure [$p(N_2)$ in Pa]. For comparison and reference to literature, the calculated patterns of Ni_3N and Ni_2N are shown.

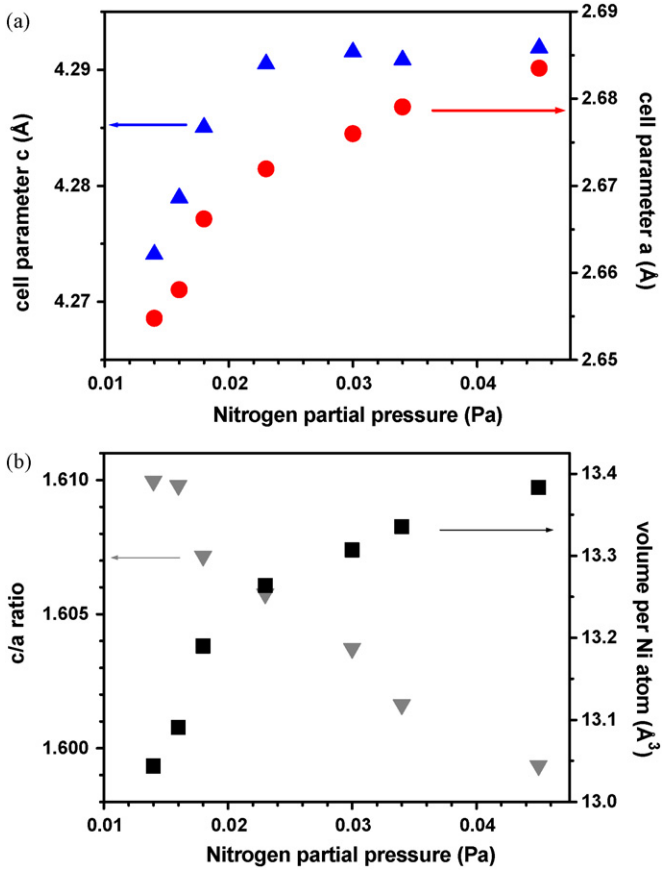

Fig. 2. (a) Cell parameters c and a for the hcp-based nickel nitride (space group $P6_322$) vs. $p(N_2)$; (b) axial ratio c/a and the volume V per nickel atom vs. $p(N_2)$.

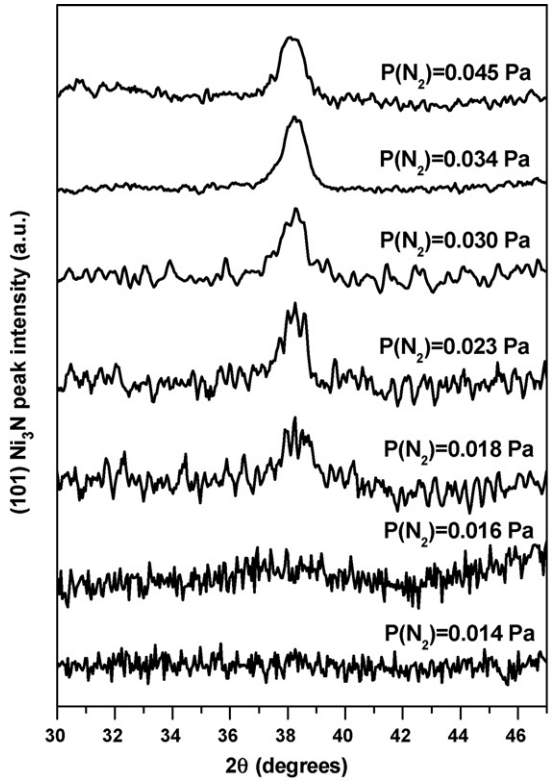

Fig. 3. The (1 0 1) diffraction peak behavior for different nitrogen partial pressures.

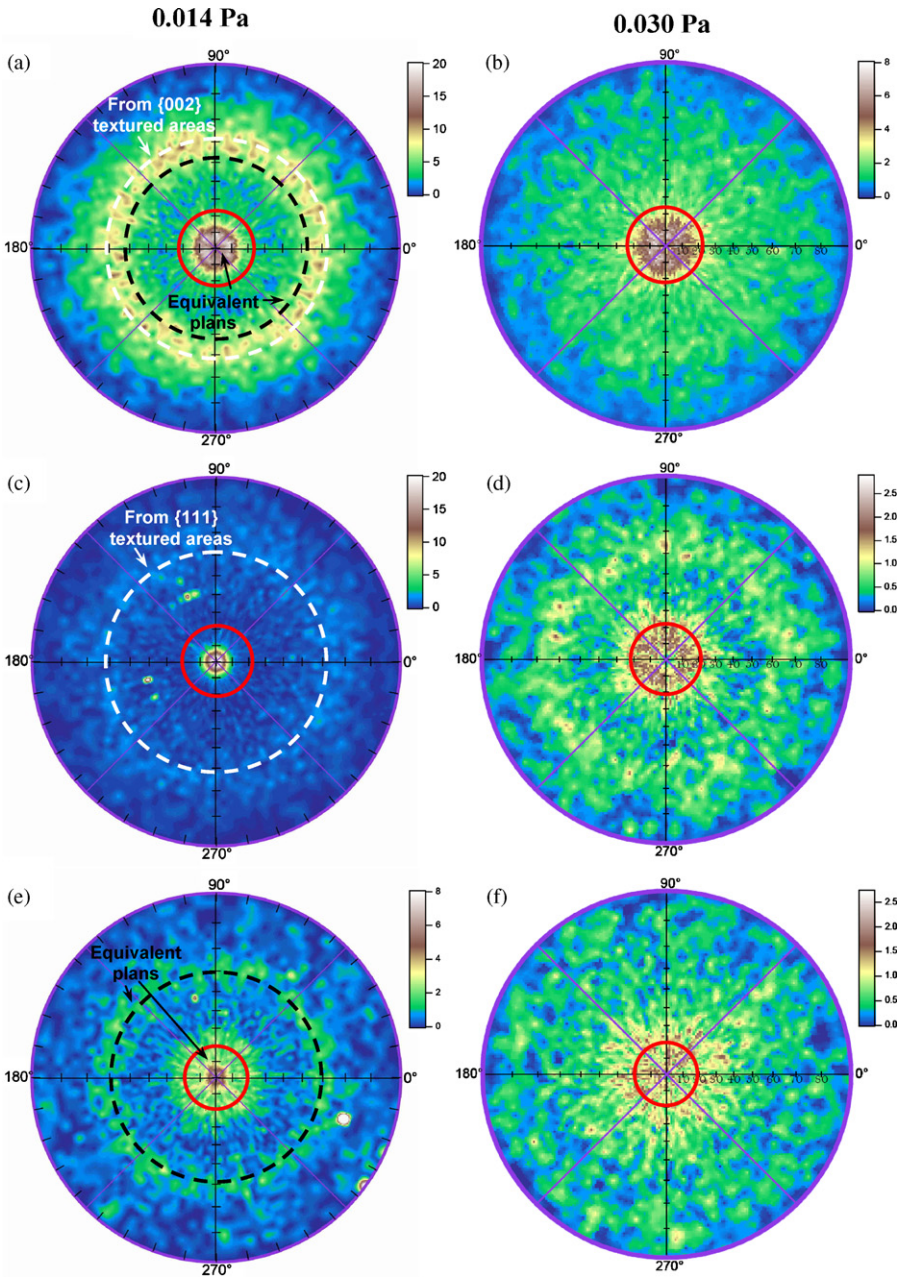

Fig. 4. Pole figures ($\lambda = 1.5418$ Å) for nickel nitrides when deposited under $p(N_2) = 0.14$ and 0.030 Pa, respectively, (a) and (b) for the (1 1 1) line with $2\theta = 44.6°$; (c) and (d) for the (0 0 2) line with $2\theta = 41.76°$; (e) and (f) for the (1 1 0) line with $2\theta = 39.04°$.

the calculated values of their corresponding theoretical diffraction patterns. This is due to preferential orientations of layer crystallites, particularly effective for layers realized under pressure lower than 0.023 Pa. The study of the texture orientation distributions is presented in the next paragraph.

A specific analysis of nitrogen richest layers, e.g. Ni_2N and their related properties, will be discussed in a forthcoming paper.

Earlier works, as for instance in Ref. [6], show that Ni_3N crystallizes in hcp sublattice structure (SG $P6_322$) with unit cell parameter $a_3 \sim 4.621$ Å and $c_3 \sim 4.304$ Å. Using a profile analysis method we have determined the unit cell parameters of Ni_3N for each synthesis pressure from corresponding diffraction patterns as reported, e.g. in Fig. 1. To easy comparisons between the Ni–N and Fe–N systems [15], we have used reduced unit cell parameters such as $a = a_3/\sqrt{3}$ and $c = c_3$. Fig. 2a shows the variation of these parameters versus $p(N_2)$. The a and c cell parameter both increase for synthesis pressure up to 0.023 Pa and reveal a tendency to saturate for higher pressure. The unit cell volume per Ni atom as shown in Fig. 2b shows a similar behavior, contrarily to the c/a ratio which exhibits a linear decrease when increases $p(N_2)$. These variations of unit cell parameters and c/a ratio are very close to what is reported in Ref. [15] for the Fe–N system where a continuous variation of stoichiometry was reported to take place from $Fe_{\sim 4}N$ to $Fe_{\sim 2}N$, as described under the frame of the ε-Fe_3N hcp structure (SG $P6_3/mmc$). Effectively, in the hexagonal system the c/a ratio decreases linearly with the nitrogen content and the unit cell parameters, a and c, both increase and start to saturate just before the emergence of the ζ-Fe_2N phase (SG $I4/mmm$) at highest nitrogen content (>49.5% Fe atoms).

Here, the behavior of the "superlattice" Bragg peak (1 0 1) of ε-Ni_3N as shown in Fig. 3, reveals that under high $p(N_2)$ synthesis pressure, the Ni_3N stoichiometry is made stable. The (1 0 1) and corresponding Bragg peaks are related to the ordered occupancy of specific Fe interstitial sites – the (2c) interstices in SG $P6_322$ – by N atoms. If the behavior of the Ni–N and Fe–N system were similar,

the N atom concentration close to 50% Ni atoms (∼a stoichiometry close to Ni_2N) could be reached without changing the Ni atoms arrangement (hypothetic hexagonal Ni_2N). According to the pioneer work of Jack [15], this would be done by adding N atoms in an ordered way, on half the (2b) sites of the $P6_322$ structure. For a better description of such hypothetic ε-Ni_2N structure, one may use the lower symmetry SG $P312$ to make simpler the discussion on interstitial site occupancy by nitrogen. In this later space group, ε-Ni_3N could be described from Ni atoms on the (6l) sites with coordinates (0,5/6,1/4) and N atoms on the (1d) site (1/3,2/3,1/2) and (1e) site (2/3,1/3,0). To describe "ε-Ni_2N", only N atoms have to be inserted in the (1a) (0,0,0) sites. Without any inserted nitrogen in the Ni lattice, the (1 0 1) peak intensity is zero. Filling the interstitial sites (1d) and (1e) in order to reach the Ni_3N stoichiometry, numerical simulation results in an increase of the calculated (1 0 1) Bragg peak intensity. Besides, filling the (1a) site with nitrogen to reach the Ni_2N stoichiometry, results as well in a much marked increase of the (1 0 1) Bragg peak. Therefore, maximization of the (1 0 1) line intensity, as experimentally observed when $p(N_2)$ increases, could be due to either a complete filling with nitrogen of the (1d) and (1e) sites to form ε-Ni_3N or the complete filling of the (1d), (1e) and (1a) interstices to get the N-richest Ni_2N.

Unfortunately the high degree of texture of the layers (as discussed later) prevents using the intensity of the (1 0 1) and other related Bragg peaks to quantify the nitrogen content of the different nickel nitrides. Nevertheless, if maximization of the (1 0 1) Bragg peak had resulted in an almost saturation of the (1a) (0,0,0) interstitial site, i.e. the formation of a hypothetical "ε-$Ni_2N_{1-\varepsilon}$" type compound, addition of a few N atoms when increasing $p(N_2)$ could be sufficient to stabilize definitively tetragonal Ni_2N layers. However, such a transformation was not observed, effectively. All these considerations are in good agreement with a rather recent neutron diffraction analysis of the N atom ordering in Ni_3N (SG $P6_322$) [16]. By increasing temperature, the authors of the study state on the impossibility for N atoms to migrate from a (1c) ordered site occupancy to a disordered (1b) site configuration, thus concluding that the Ni_3N type compound is limited to the 3:1 stoichiometry. Thus, we can assert that maximization of the (1 0 1) Bragg peak is due to the total filling of the (1d) and (1e) sites, corresponding to the Ni_3N stoichiometry, and accordingly on an improbable significant occupancy of the (0,0,0) sites to form a hexagonal "ε-$Ni_2N_{1-\varepsilon}$". According to these considerations, our sample with a 3:1 stoichiometry as deposited under $p(N_2) = 0.030$ Pa, without any trace of tetragonal Ni_2N, was retained to characterize magnetically Ni_3N.

3.2. Microstructure characteristics

We have performed systematically pole figure measurements on all the samples in order to understand the behavior of the relative intensities of the main series of peaks {1 1 1}, {0 0 2} and {1 1 0} in terms of crystal growth. Fig. 4 shows the results for nitrogen partial pressures synthesis of 0.014 and 0.030 Pa. On these figures, each position of coordinates (Ψ, θ) represents an orientation for the considered plan. It is worth to note that the distribution of orientations of the {1 1 1}, {0 0 2} and {1 1 0} plans is concentrated around the angle $\Psi = 0^\circ$ which corresponds to the effective growing direction of the film. Hence, it is possible to conclude that the deposits have a monocrystalline columnar microstructure. So the deposit is constituted from different columns, each one having its own orientation within the deposit. In the X-ray diffraction patterns taken at grazing incidence, a diffraction peak at the 2θ angle corresponds to those plans at θ angle to the normal axis of the layer. Thus, the intensity of the diffraction peak corresponds to the integrated intensity of the pole figure measured on a circle of diameter θ. These circles are represented (in red) in Fig. 4. For a sample synthesized under a N_2 pressure of 0.014 Pa, Fig. 4c shows a sharp (0 0 2) plan distribution perpendicular to the layer. Conversely the very low intensity peak measured at $\theta = 20.73^\circ$ as shown in this figure (red circle) corresponds to a quasi-absence of the (0 0 2) peak in the diffraction pattern. For films synthesized under higher N_2 pressures, e.g. 0.030 Pa, as displayed in Fig. 4b, the intensity of the $\theta = 0^\circ$ peaks for the (0 0 2) plans is almost eight times lower comparison made to the previous type samples as synthesized under 0.014 Pa N_2 pressure. Nevertheless, a texture effect is still present in such layers. In addition, the {0 0 2} and {1 1 0} oriented columnar sketches tend to disappear faster than the {1 1 1} one when the pressure of synthesis is increased. Furthermore, specific texture effects for Ni_2N composition stabilized in the films are still observed when deposits are realized under a N_2 pressure higher than 0.034 Pa, as well as in the case of pure nickel deposits.

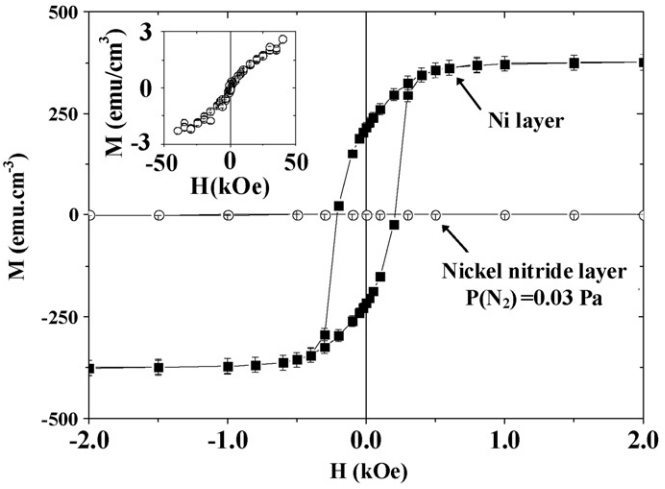

Fig. 5. Magnetization vs. field measured at 4.2 K in a nickel film and a nickel nitride deposited under $p(N_2) = 0.030$ Pa. In the inset: M(H) cycle measured in a larger magnetic fields range (±50 kOe) for the nitride layer.

4. Magnetic properties

4.1. Magnetization measurements

M(H) typical loops realized by SQUID measurements at 4.2 K, for both a Ni nitride layer as deposited under $p(N_2) = 0.030$ Pa and a layer of pure Ni with a same thickness (∼100 nm), are shown in Fig. 5. In the inset of Fig. 5, the magnetic cycle of the Ni_3N layer is added for a larger range of magnetic fields (±50 kOe). As expected, the Ni film is of soft ferromagnetic type with a rather low coercitive field close to 220 Oe, the remanent magnetization reaching 57%, a saturation magnetization of $M_{sat} = 380$ emu/cm^3 (∼57.5 emu/g) close to the theoretical value and a saturation field (magnetization at 95% of M_{sat}) of 550 Oe.

The Ni_3N layer does not exhibit any significant ferromagnetic polarization and the persistence of a loop with a weak signal (2–3 emu/cm^3) and low saturation, as seen in the inset of Fig. 5, may be attributed to residual but almost paramagnetic impurities either in the layer or at interface with the substrate (Ni/Si interface effects). Similar results were obtained for the series of nitride layers with a pressure $p(N_2)$ comprised between 0.014 and 0.045 Pa at synthesis, showing as well the non-magnetic state of the Ni_2N nickel nitride. We have also observed similar results in a Ni_3N film elaborated by plasma-based ion implantation [17] where a weak ferromagnetic signal of the nitride films has been assigned to residual non-nitrided Ni. In the later reference, the ratio $R = M_{sat}(Ni_3N)/M_{sat}(Ni)$ reaches 1/57 whereas R is minimized down to 1/400 only for the present deposits we have synthesized. Besides in Ref. [8], it is said that

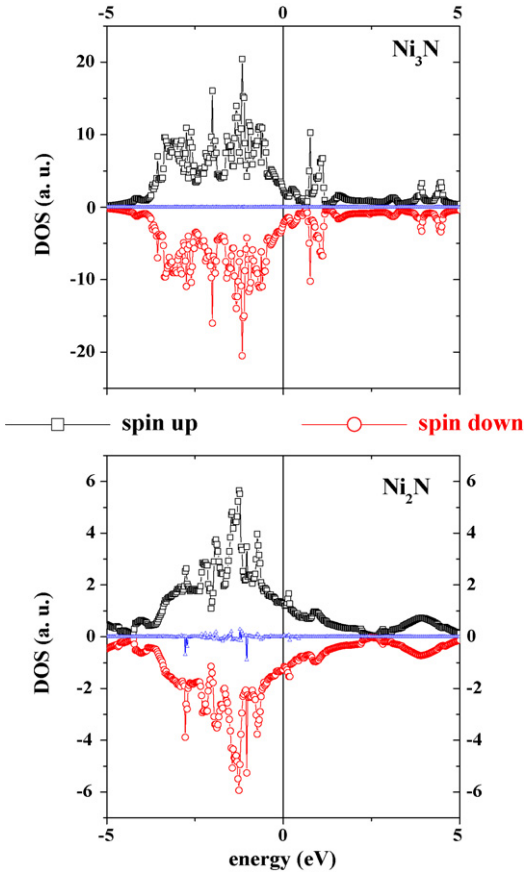

Fig. 6. Density of states (a) of Ni_3N and (b) Ni_2N for nitride layers.

local Ni_3N precipitates lead evidence to some weak magnetization contribution, this effects being more probably due to regions Ni-containing precipitates in agreement with results of the present study.

4.2. Theoretical magnetic properties

A Full Potential Linearized Augmented Plane Wave (FLAPW) analysis [18] was used to compare the present experimental results to the theoretical magnetic states of both Ni_3N and Ni_2N. The analysis consists in Differential Functional Theory (DFT) calculations using the Local Density Approximation (LDA) taking wave functions as a basis. The Kohn–Sham equation and energy functional [19] were evaluated consistently. The FLAPW calculations were performed using the crystal structure parameters derived from the here determined X-ray measurements, e.g. for samples deposited under $p(N_2) = 0.030$ Pa. The results of band structure calculations with a spin polarized potential when assuming a ferromagnetic state of Ni_3N lead to determine the total Density of States (DOS), the partial DOS and the l-decomposed DOS on the Ni site. Examinations of all these DOS and especially the total DOS provides evidence that no magnetic polarization is found indicating particularly no localized moment on the Ni atom in both nitrides Ni_3N and Ni_2N. Two theoretical curves of DOS versus energy are given in Fig. 6a for Ni_3N and Fig. 6b for Ni_2N. Therefore, calculations also show no DOS polarization can be found in the interstitial space. Hence, one can conclude that neither itinerant nor localized magnetism is present proving a full paramagnetic state of these nitride layers for both the studied binary nitrides. Consistent results were already mentioned in different studies related to the NiN system by using FLAPW band calculations [20] or a self-consistent Full-Potential Linear Muffin-Tin Orbital (FP-LMTO) method [21]. However, in the later studies the cell parameter was chosen as corresponding to a NaCl-type structure a situation which differs from the present structural analysis. Whatever are the bases of the theoretical investigation analysis, no magnetic ordered state was determined in Ni–N binary systems. However, here we have established with no ambiguity a non-magnetic state of Ni_3N from both theoretical and experimental results.

5. Conclusion

Nickel nitride layers were deposited by reactive sputtering assisted by microwaves multidipolar plasma technique. By varying the nitrogen partial pressure in the argon–nitrogen gas mixture, nickel nitride layers with different compositions were synthesized. At medium nitrogen pressure, a stoichiometric Ni_3N was synthesized. At higher pressure, a mixture of Ni_2N and Ni_3N is synthesized. Magnetic measurement performed on this sample shows the paramagnetic behavior of both Ni_3N and Ni_2N. This result is confirmed by a theoretical study performed using the FLAPW method.

References

[1] J.N. Zhou, A. Rar, D. Otte, J.A. Barnard, J. Appl. Phys. 88 (2000) 1880.
[2] P.R. Cantwell, U.J. Gibson, D.A. Allwood, H.A.M. Macleod, J. Appl. Phys. 100 (2006) 093910.
[3] J. Pérez-Rigueiro, C. Jiménez, R. Pérez-Casero, J.M. Martínez-Duart, J. Appl. Phys. 81 (1997) 781.
[4] V. Lingwal, N.S. Panwar, J. Appl. Phys. 97 (2005) 104902.
[5] R. Dubey, A. Gupta, J. Appl. Phys. 98 (2005) 083903.
[6] R. Juza, W. Sachze, Z. Anorg. Allg. Chem. 251 (1943) 201.
[7] G.J.W. Dorman, M. Sikkens, Thin Solid Films 105 (1983) 251.
[8] I.M. Neklyudov, A.N. Morozov, Physica B 350 (2004) 325.
[9] D. Vempaire, S. Miraglia, A. Sulpice, et al., J. Magn. Magn. Mater. 272 (2004) E843–E844.
[10] T. Takamori, K.K. Shih, D.B. Dove, R.W. Nywening, M.E. Re, J. App. Phys. 68 (1990) 2192.
[11] L. Maya, T. Thundat, J.R. Thompson, R.J. Stevenson, App. Phys. Lett. 67 (1995) 3034.
[12] N.S. Gajbhiye, R.S. Ningthoujam, J. Weissmuller, Phys. Stat. Sol. (a) 189 (2002) 691.
[13] B.D. Cullity, Introduction to Magnetic Materials, Addison–Wesley, Reading, MA, 1972.
[14] S. Béchu, O. Maulat, A. Lacoste, Y. Arnal, D. Vempaire, J. Pelletier, Surf. Coat. Technol. 186 (2004) 170.
[15] K.H. Jack, Acta Cryst. 5 (1952) 404.
[16] A. Leineweber, H. Jacobs, S. Hull, Inorg. Chem. 40 (2001) 5818.
[17] D. Vempaire, J. Pelletier, A. Lacoste, S. Béchu, J. Sirou, S. Miraglia, D. Fruchart, Plasma Phys. Control. Fusion 47 (2005) A153.
[18] P. Blaha, K. Schwartz, P. Sorantin, S.B. Trikey, Comput. Phys. Commun. 59 (1990) 39–49.
[19] W. Kohn, L.J. Sham, Phys. Rev. 140 (1965) A1133.
[20] H. Shimizu, M. Shirai, N. Suzuki, J. Phys. Soc. Jpn. 66 (1997) 3147.
[21] W. Hong-Bo, X. De-Sheng Chi, Phys. Lett. 21 (2004) 1612.